Mon. Not. R. Astron. Soc. **386,** 1487–1502 (2008) doi:10.1111/j.1365-2966.2008.13112.x

Probing the properties of convective cores through g modes: high-order g modes in SPB and γ Doradus stars

Andrea Miglio, Josefina Montalbán,★ Arlette Noels and Patrick Eggenberger
Institut d'Astrophysique et de Géophysique de l'Université de Liège, Allée du 6 Août, 17 B-4000 Liège, Belgium

Accepted 2008 February 15. Received 2008 February 14; in original form 2007 July 2

ABSTRACT

In main-sequence stars, the periods of high-order gravity modes are sensitive probes of stellar cores and, in particular, of the chemical composition gradient that develops near the outer edge of the convective core. We present an analytical approximation of high-order g modes that takes into account the effect of the μ gradient near the core. We show that in main-sequence models, similarly to the case of white dwarfs, the periods of high-order gravity modes are accurately described by a uniform period spacing superposed to an oscillatory component. The periodicity and amplitude of such component are related, respectively, to the location and sharpness of the μ gradient.

We investigate the properties of high-order gravity modes for stellar models in a mass domain range between 1 and 10 $M_\odot$, and the effects of the stellar mass, evolutionary state and extra-mixing processes on period spacing features. In particular, we show that for models of a typical Slowly Pulsating B (SPB) star, a chemical mixing that could likely be induced by the slow rotation observed in these stars is able to significantly change the g-mode spectra of the equilibrium model. Prospects and challenges for the asteroseismology of γ Doradus and SPB stars are also discussed.

Key words: stars: evolution – stars: interiors – stars: oscillations – stars: variables: other.

1 INTRODUCTION

It is well known that a stratification in the chemical composition of stellar models directly influences the properties of gravity modes. The signatures of chemical stratifications have been extensively investigated theoretically, and observed, in pulsating white dwarfs (see e.g. Kawaler 1995, for a review). The influence of chemical composition gradients on g modes in main-sequence stars has been partly addressed and suggested in the works by Berthomieu & Provost (1988) and Dziembowski, Moskalik & Pamyatnykh (1993). Inspired by these works and following the approach of Berthomieu & Provost (1988) and Brassard et al. (1992), we study the properties of high-order, low-degree gravity modes in main-sequence stellar models.

High-order gravity modes are observed in two classes of main-sequence stars: γ Doradus and Slowly Pulsating B (SPB) stars. The former are main-sequence stars with masses around 1.5 $M_\odot$ (see e.g. Guzik et al. 2000) that show both photometric and line profile variations. Their spectral class is A7–F5 and their effective temperature is between 7200–7700 K on the zero-age main sequence (ZAMS) and 6900–7500 K above it (Handler 1999). γ Dor stars are multiperiodic oscillators with periods between 8 h and 3 d (high-order g modes). The modulation of the radiative flux by convection at the base of the convective envelope was proposed as the excitation mechanism for such stars (see e.g. Guzik et al. 2000; Dupret et al. 2004).

SPB stars are multiperiodic main-sequence stars with masses from about 3 to 8 $M_\odot$ and spectral-type B3–B8 (Waelkens 1991). High-order g modes of periods typically between 1 and 3 d are found to be excited by the κ-mechanism acting in the region of the metal opacity bump located at $T \sim 2 \times 10^5$ K in the stellar interior (see e.g. Dziembowski et al. 1993). Recent observations (see Jerzykiewicz et al. 2005; Chapellier et al. 2006; Handler et al. 2006) and theoretical instability analysis (Pamyatnykh 1999; Miglio, Montalbán & Dupret 2007) also suggest high-order g modes being excited in a large fraction of the more massive β Cephei pulsators: the seismic modelling of these hybrid pulsators looks very promising as it would benefit from the information on the internal structure carried by both low-order p and low-order g modes (β Cephei type oscillation modes) and high-order g modes (SPB-type pulsation).

The seismic modelling of γ Doradus and SPB stars is a formidable task to undertake. The frequencies of high-order g modes are in fact closely spaced and can be severely perturbed by the effects of rotation (see e.g. Dintrans & Rieutord 2000; Suárez et al. 2005). None the less, the high scientific interest of these classes of pulsators has driven efforts in both the observational and theoretical domain. Besides systematic photometric and spectroscopic ground-based surveys carried out on γ Dor (see Mathias et al. 2004) and SPB stars (see De Cat & Aerts 2002), the long and uninterrupted photometric observations planned with COnvection, ROtation & Planetary

★E-mail: j.montalban@ulg.ac.be

Transits (CoRoT; Baglin et al. 2006; Mathias et al. 2006) will allow to significantly increase the number and accuracy of the observed frequencies.

On the theoretical side, as suggested by Suárez et al. (2005) in the case of γ Dor stars, a seismic analysis becomes feasible for slowly rotating targets. In these favourable cases, the first-order asymptotic approximation (Tassoul 1980) can be used as a tool to derive the buoyancy radius of the star (see Moya et al. 2005) from the observed frequencies. Nevertheless, the g-mode spectra of these stars contain much more information on the internal structure of the star. In this paper, we describe in detail the information content carried by the periods of high-order g modes, and show that the effect of chemical composition gradients can be easily included as a refinement of the asymptotic approximation of Tassoul (1980).

After an introduction to the properties of gravity modes in main-sequence stars (Section 2), we present in Section 3 the analytical approximation of high-order g-mode frequencies that will be used in the subsequent sections. In Section 4, we describe the properties of numerically computed g-mode frequencies in main-sequence stars in the mass domain 1–10 $M_\odot$. The effect of adding extra-mixing at the outer edge of the convective core (rotationally induced turbulence, overshooting, diffusion) is investigated in Section 4.2. In Section 5, we estimate how the effects of rotation and of current observational limitations affect asteroseismology of main-sequence high-order g-modes pulsators. A summary is finally given in Section 6.

2 THE PROPERTIES OF TRAPPED g MODES

As is well known, the period spectrum of gravity modes is determined by the spatial distribution of the Brunt–Väisälä frequency (N) which is defined as

$$N^2 = g\left(\frac{1}{\Gamma_1 p}\frac{\mathrm{d}p}{\mathrm{d}r} - \frac{1}{\rho}\frac{\mathrm{d}\rho}{\mathrm{d}r}\right). \quad (1)$$

N can be approximated, assuming the ideal gas law for a fully ionized gas, as

$$N^2 \simeq \frac{g^2\rho}{p}(\nabla_{\rm ad} - \nabla + \nabla_\mu), \quad (2)$$

where

$$\nabla = \frac{\mathrm{d}\ln T}{\mathrm{d}\ln p}, \quad \nabla_{\rm ad} = \left(\frac{\partial \ln T}{\partial \ln p}\right)_{\rm ad} \text{ and } \nabla_\mu = \frac{\mathrm{d}\ln\mu}{\mathrm{d}\ln p}. \quad (3)$$

The term ∇_μ gives the explicit contribution of a change of chemical composition to N. The first-order asymptotic approximation developed by Tassoul (1980) shows that, in the case of a model that consists of an inner convective core and an outer radiative envelope (we refer to the work by Tassoul 1980, for a complete analysis of other possible cases), the periods of low-degree, high-order g modes are given by

$$P_k = \frac{\pi^2}{L\int_{x_0}^1 \frac{|N|}{x}\mathrm{d}x}(2k + n_{\rm e}), \quad (4)$$

where $L = [\ell(\ell+1)]^{1/2}$ (with ℓ the mode degree), $n_{\rm e}$ the effective polytropic index of the surface layer, x the normalized radius and x_0 corresponds to the boundary of the convective core. In order to avoid confusion with $n_{\rm e}$, the radial order of g modes is represented by k.

Following equation (4), the periods are asymptotically equally spaced in k and the spacing decreases with increasing L. It is therefore natural to introduce, in analogy to the large frequency separation of p modes, the *period spacing* of gravity modes, defined as

$$\Delta P = P_{k+1} - P_k. \quad (5)$$

In the following sections, we will show that deviations from a constant ΔP contain information on the chemical composition gradient left by a convective core evolving on the main sequence.

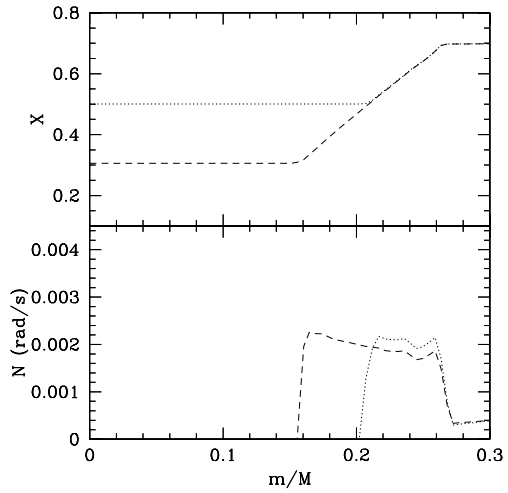

Figure 1. Upper panel: hydrogen abundance in the core of 6 $M_\odot$ models on the main sequence. $X_{\rm c} \simeq 0.5$ (dotted line) and at $X_{\rm c} \simeq 0.3$ (dashed line). The convective core recedes during the evolution and leaves behind a chemical composition gradient. Lower panel: buoyancy frequency N as a function of the normalized mass.

We consider as a first example two models of a 6 $M_\odot$ star evolving on the main sequence. The behaviour of N and of the chemical composition profile is represented in Fig. 1. The convective core is fully mixed and, therefore, the composition is uniform ($\nabla_\mu = 0$). However, in stars in this mass range, the convective core shrinks during the evolution, leaving behind a steep gradient in the hydrogen abundance X. This causes a sharp peak in ∇_μ and in N: does this feature leave a clear signature in the properties of g modes? This question was addressed by Brassard et al. (1991) while studying the seismic effects of compositional layering in white dwarfs. The authors found that a sharp feature in the buoyancy frequency could lead to a resonance condition that may trap modes in different regions of the model.

A first indicator of such a trapping is the behaviour of $\langle x\rangle$ defined by

$$\langle x\rangle = \frac{\int_0^1 x|\boldsymbol{\delta r}|^2\,\mathrm{d}m}{\int_0^1 |\boldsymbol{\delta r}|^2\,\mathrm{d}m}, \quad (6)$$

where $x = r/R$ and $\boldsymbol{\delta r}$ is the total displacement vector. As shown in Fig. 2, modes of different radial order k are *periodically confined* closer to the centre of the star.

In Fig. 3, we show the behaviour of the eigenfunctions for modes of radial orders around a trapped mode: the partly trapped mode has, compared to 'neighbour' modes, a larger amplitude in the region of mean molecular weight gradient.

In white dwarfs, it has been theoretically predicted and observed (see e.g. the recent work of Metcalfe, Montgomery & Kawaler 2003) that the period spacing $\Delta P(k) = P_{k+1} - P_k$ is not constant, contrary to what is predicted by the first-order asymptotic approximation of gravity modes. This has been interpreted as the signature of chemical composition gradients in the envelope and in the core of the star. In analogy with the case of white dwarfs, in models with a

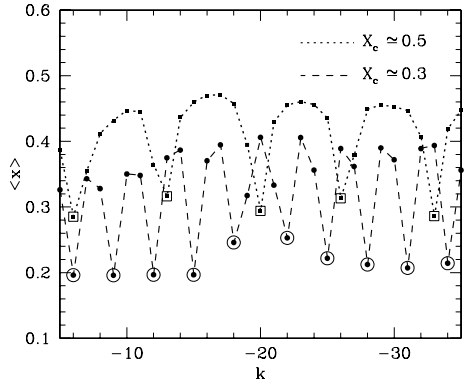

Figure 2. $\langle x \rangle$ for 6 $M_\odot$ models on the main sequence at two different points in the evolution: $X_c \simeq 0.5$ (dotted lines) and at $X_c \simeq 0.3$ (dashed line). Modes of different radial order are periodically trapped in the region of chemical composition gradient. Trapped modes are marked with open symbols.

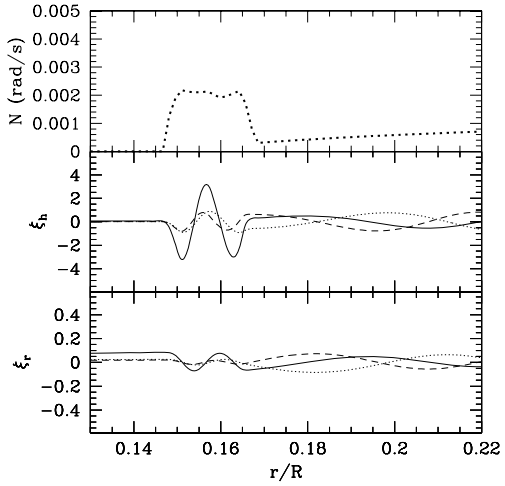

Figure 3. We consider a 6 $M_\odot$ model with $X_c \simeq 0.5$. Upper panel: N against fractional radius. Central panel: horizontal component of the displacement for three $\ell = 1$ gravity modes of radial order 18 (dotted line), 20 (continuous line) and 22 (dashed line). The eigenfunction corresponding to $k = 20$ is partly trapped in the region of mean molecular weight where the sharp variation of N is located. Lower panel: as in the central panel, this time the radial displacement is shown. The eigenfunctions corresponding to different modes are normalized to have the same total pulsation energy.

convective core, we expect the formation of a *non-uniform period distribution*; this is in fact the case as is presented in Fig. 4. In that figure, we plot the period spacing derived by using the adiabatic oscillation code LOSC (Scuflaire et al. 2007a) for models of 6 $M_\odot$ at two different stages in the main-sequence evolution. The period spacing presents clear deviations from the uniformity that would be expected in a model without sharp variations in N. How these deviations are related to the characteristics of the chemical composition gradients will be studied in the following sections.

3 APPROXIMATE ANALYTICAL EXPRESSION OF G-MODES PERIOD SPACING

In this section, we derive two approximate expressions that relate deviations from a uniform period distribution to the characteristics of the μ-gradient region. These simplified expressions could also represent a useful tool to give a direct interpretation of an observed

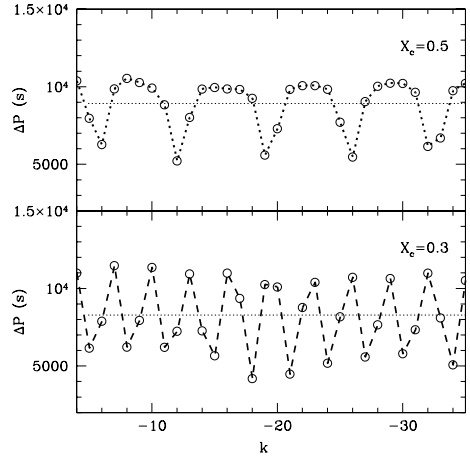

Figure 4. Period spacing for the same 6 $M_\odot$ models as in Fig. 2. The periods of the components (in terms of k) are approximately 7 and 3. Horizontal dotted lines represent constant period spacing predicted by the asymptotic approximation (equation 4).

period spectrum. Though a first description of these approximated expressions was outlined in Miglio (2006) and in Miglio, Montalbán & Noels (2006), we present here a more detailed analysis.

We recall that deviations from the asymptotic expressions of the frequencies of high-order pressure modes have been widely studied in the context of helioseismology. The oscillatory features in the oscillation spectrum of solar oscillation modes allowed modes to infer the properties of localized variations of the solar structure, for example, at the base of the convective envelope and in the second helium ionization region (see e.g. Gough 1990; Christensen-Dalsgaard, Gough & Thompson 1991; Monteiro, Christensen-Dalsgaard & Thompson 1994; Basu & Antia 1995; Monteiro & Thompson 2005; Houdek & Gough 2007).

3.1 Variational principle

A first and simple approach to the problem is to make use of the variational principle for adiabatic stellar oscillations (see e.g. Unno et al. 1989). The effect of a sharp feature in the model (a chemical composition gradient, for instance) can be estimated from the periodic signature in ΔP, defined as the difference between the periods of the star showing such a sharp variation and the periods of an otherwise fictitious smooth model.

We consider a model with a radiative envelope and a convective core whose boundary is located at a normalized radius x_0. N_- and N_+ are the values of the Brunt–Väisälä frequency at the outer and inner border of the μ-gradient region. We define $\alpha = (\frac{N_+}{N_-})^{1/2}$ with $N_+ \leqslant N_-$. Then, $\alpha = 1$ describes the smooth model and $\alpha \to 0$ a sharp discontinuity in N.

To obtain a first estimate of δP, we adopt (following the approach by Montgomery, Metcalfe & Winget 2003) the Cowling approximation that reduces the differential equations of stellar adiabatic oscillations to a system of the second order. Furthermore, since we deal with high-order gravity modes, the eigenfunctions are well described by their Jeffreys–Wentzel–Kramers–Brillouin approximation (see e.g. Gough 1993). We can therefore express δP as

$$\frac{\delta P_k}{P} = 2\Pi_0 \int_0^{\Pi_0^{-1}} \left(\frac{\delta N}{N}\right) \cos\left(\frac{L\ P_k}{\pi\ \Pi_x} + \frac{\pi}{2}\right) \mathrm{d}\Pi_x^{-1}, \qquad (7)$$

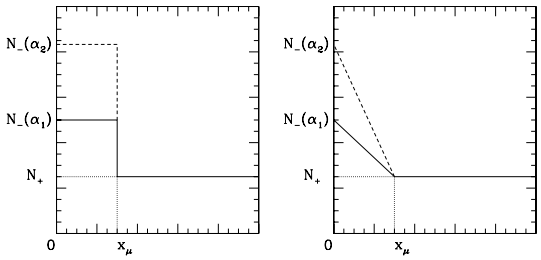

Figure 5. Left-hand panel: we model the sharp variation of N at $x = x_\mu$ by means of equation (11) for different values of α: $\alpha_1^2 = 0.5$ (continuous line), $\alpha_2^2 = 0.3$ (dashed line). Right-hand panel: a smoother variation of N is modelled following equation (15).

where $L = [\ell(\ell+1)]^{1/2}$, the local buoyancy radius is defined as

$$\Pi_x^{-1} = \int_{x_0}^{x} \frac{|N|}{x'} \mathrm{d}x', \tag{8}$$

and the total buoyancy radius as

$$\Pi_0^{-1} = \int_{x_0}^{1} \frac{|N|}{x'} \mathrm{d}x'. \tag{9}$$

The buoyancy radius of the discontinuity is then

$$\Pi_\mu^{-1} = \int_{x_0}^{x_\mu} \frac{|N|}{x'} \mathrm{d}x'. \tag{10}$$

We model the sharp feature in $\frac{\delta N}{N}$ located at $x = x_\mu$ as

$$\frac{\delta N}{N} = \frac{1-\alpha^2}{\alpha^2} H(x_\mu - x), \tag{11}$$

where $H(x)$ is the step function (see left-hand panel of Fig. 5).

Retaining only periodic terms in ΔP and integrating by parts, we obtain

$$\delta P_k \propto \frac{\Pi_0}{L} \frac{1-\alpha^2}{\alpha^2} \cos\left(\frac{L\, P_k}{\pi\, \Pi_\mu} + \frac{\pi}{2}\right). \tag{12}$$

For small δP, we can substitute the asymptotic approximation for g-modes periods derived by Tassoul (1980) in the above expression:

$$P_k = \pi^2 \frac{\Pi_0}{L}(2k + \phi'),$$

where ϕ' is a phase constant that depends on the boundary conditions of the propagation cavity (see Tassoul 1980), and find

$$\delta P_k \propto \frac{\Pi_0}{L} \frac{1-\alpha^2}{\alpha^2} \cos\left(2\pi \frac{\Pi_0}{\Pi_\mu} k + \pi \frac{\Pi_0}{\Pi_\mu} \phi' + \frac{\pi}{2}\right). \tag{13}$$

From this simple approach, we derive that the signature of a sharp feature in the Brunt–Väisälä frequency is a *sinusoidal component in the periods of oscillations*, and therefore in the period spacing, with a periodicity in terms of the radial order k given by

$$\Delta k \simeq \frac{\Pi_\mu}{\Pi_0}. \tag{14}$$

The amplitude of this sinusoidal component is proportional to the sharpness of the variation in N and does not depend on the order of the mode k.

Such a simple approach allows us to easily test the effect of having a less sharp 'glitch' in the Brunt–Väisälä frequency. We model δN (Fig. 5, right-hand panel) as a ramp function instead of a step function:

$$\frac{\delta N}{N} = \frac{1-\alpha^2}{\alpha^2} \frac{(x_\mu - x)}{x_\mu - x_0} H(x_\mu - x). \tag{15}$$

In this case, integration by parts leads to a sinusoidal component in δP_k whose *amplitude is modulated by a factor* $1/P_k$ and therefore decreases with increasing k, i.e.

$$\delta P_k \propto \frac{1}{P_k} \frac{\Pi_0}{L} \frac{1-\alpha^2}{\alpha^2} \frac{1}{\Pi_\mu^{-1}} \cos\left(2\pi \frac{\Pi_0}{\Pi_\mu} k + \pi \frac{\Pi_0}{\Pi_\mu} \phi' + \frac{\pi}{2}\right). \tag{16}$$

The information contained in the amplitude of the sinusoidal component, as will be presented in Section 4.2, is potentially very interesting. It reflects the different characteristics of the chemical composition gradient resulting, for example, from a different treatment of the mixing process in convective cores, from considering microscopic diffusion or rotationally induced mixing in the models.

Equation (13) was derived by means of a first-order perturbation of the periods neglecting changes in the eigenfunctions. This approximation is valid in the case of small variations relative to a smooth model, therefore it becomes questionable as the change of N at the edge of the convective core becomes large. A more accurate approximation is presented in the following section.

3.2 Considering the effects of the μ gradient on the eigenfunctions

We present in this section a description of mode trapping considering the change in the eigenfunctions due to a sharp feature in N. As a second step, we derive the effects on the periods of g modes.

Brassard et al. (1992) studied the problem of mode trapping in μ-gradient regions inside white dwarfs. In this section, we proceed as Brassard et al. (1992), applying the asymptotic theory as developed in Tassoul (1980) to the typical structure of an intermediate-mass star on the main sequence.

Tassoul (1980), assuming the Cowling approximation, provided asymptotic solutions for the propagation of high-order g modes in convective and radiative regions, located in different parts of the star. In order to generalize the expression for these solutions, she introduced two functions S_1 and S_2 related to the radial displacement (ξ_r) and pressure perturbation (p') as follows:

$$\sigma^2 \xi_\mathrm{r} = \rho^{-1/2} x^{-2} |\phi|^{-1/4} S_1 \tag{17}$$

and

$$\sigma\, \ell(\ell+1) p'/\rho = \rho^{-1/2} |\phi|^{1/4} S_2\ , \tag{18}$$

where x is the normalized radius, σ the angular frequency of the oscillation and

$$\phi = \frac{\ell(\ell+1) N^2}{x^2}. \tag{19}$$

The expressions for S_1, S_2 for different propagation regions are given in equations [T79] to [T97].[1]

The only difference from the derivation of Brassard et al. (1992), who assumed an entirely radiative model, is that here we consider a model that consists of a convective core and a radiative envelope. The solutions should then be described by [T80] close to the centre, [T96] in the convective core (x_0), [T97] in the radiative region with [T82] close to the surface (where the structure of the surface layers of the model is described by an effective polytropic index n_e).

Now, as explained in Fig. 6, we assume that at $x = x_\mu$ in the radiative zone there is a sharp variation of N due to a μ gradient and, as in the previous section, we model it as a discontinuity weighted by α, where $\alpha = (N_+/N_-)^{1/2}$ (see equation 11).

[1] Henceforth on [Ti] indicates equation number i in the paper by Tassoul (1980).

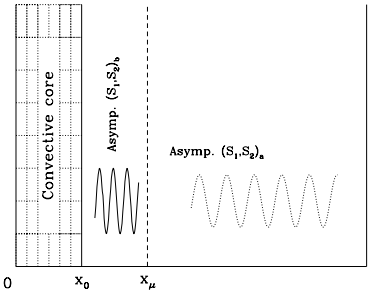

Figure 6. A schematic view of the simplified model we consider. The radiative region outside the convective core ($x > x_0$) is divided in two zones: one below and the other above the discontinuity in N located at $x = x_\mu$. In each of these regions, we consider the asymptotic expressions for the eigenfunctions that are then joined continuously at $x = x_\mu$.

We define $\lambda = \sigma^{-1}$,

$$v_0(x) = L \int_x^1 \frac{|N|}{x'}\,\mathrm{d}x' = L\left(\Pi_0^{-1} - \Pi_x^{-1}\right)$$

and $v_1(x) = L \int_{x_0}^{x} \frac{|N|}{x'}\,\mathrm{d}x' = L\Pi_x^{-1}.$

For large values of λv_0 and λv_1, we can write the eigenfunctions in the radiative region above the discontinuity at x_μ as

$$S_{1a} \propto k_o \sin(A) \quad \text{and} \quad S_{2a} \propto -k_o \cos(A), \tag{20}$$

and in the $\nabla\mu$ region below the discontinuity we have

$$S_{1b} \propto k_1 \cos(B) \quad \text{and} \quad S_{2b} \propto -k_1 \sin(B)\,, \tag{21}$$

where

$$A = \lambda v_0(x) - n_e\frac{\pi}{2} - \frac{\pi}{4}, \qquad B = \lambda v_1(x) - \frac{\pi}{4}, \tag{22}$$

and k_0 and k_1 are arbitrary constants. Note that A and B are functions of x.

The eigenfrequencies are now obtained by continuously matching the individual solutions in their common domain of validity. In particular, imposing the continuity of p' and ξ_r at the location of the discontinuity in N we obtain the following conditions (as in Brassard et al. 1992):

$$S_1^+ = \alpha S_1^-, \tag{23}$$

$$S_2^+ \alpha = S_2^-, \tag{24}$$

where $S_{1,2}$ is evaluated above ($S_{1,2}^+$) and below ($S_{1,2}^-$) $x = x_\mu$.

This finally leads to a condition on the eigenfrequencies $1/\lambda$:

$$\cos(A + B) = \frac{1-\alpha^2}{1+\alpha^2}\cos(A - B), \tag{25}$$

with A and B (equation 22) evaluated at $x = x_\mu$, this condition can also be explicitly written as

$$\cos\left(\lambda\frac{L}{\Pi_0} - \frac{n_e\pi}{2} - \frac{\pi}{2}\right) = \frac{1-\alpha^2}{1+\alpha^2}\cos\left(\lambda L\left[\frac{1}{\Pi_0} - \frac{2}{\Pi_\mu}\right] - \frac{n_e\pi}{2}\right). \tag{26}$$

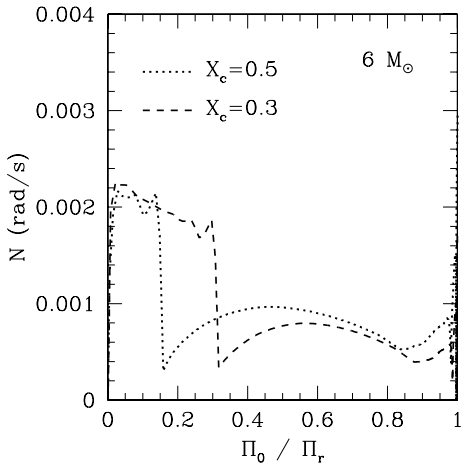

Figure 7. The Brunt–Väisälä frequency versus Π_0/Π_r for $6\,M_\odot$ models with $X_c \simeq 0.5$ (dotted line) and $X_c \simeq 0.3$ (dashed line).

3.2.1 Further approximations

A first extreme case for equation (26) is that corresponding to $\alpha = 1$, i.e. no discontinuities in the Brunt–Väisälä frequency. In this case, equation (25) immediately leads to the condition $\cos(A + B) = 0$ and therefore to the uniformly spaced period spectrum predicted by Tassoul's first-order approximation:

$$P_k = \pi^2\frac{\Pi_0}{L}(2k + n_e). \tag{27}$$

Another extreme situation is $\alpha \to 0$, in this case N is so large in the μ-gradient region that all the modes are trapped there; the periods of 'perfectly trapped' modes are then:

$$P_n = \left(n + \frac{1}{4}\right)2\pi^2\frac{\Pi_\mu}{L}, \tag{28}$$

where $n = (1, 2, 3, \ldots)$.

The interval (in terms of radial order k) Δk between two consecutive trapped modes ($\Delta n = 1$) can be obtained combining equations (27) and (28) (see also Brassard et al. 1992), and is roughly given by

$$\Delta k \simeq \frac{\Pi_\mu}{\Pi_0}, \tag{29}$$

which corresponds to equation (14).

We choose the $6\,M_\odot$ models considered in Section 2 to compare the g-mode period spacings predicted by equations (14) and (26), with the results obtained from the frequencies computed with an adiabatic oscillation code.

Equation (14) relates the period of the oscillatory component in the period spacing ΔP to the location of the sharp variation in N. In Fig. 4, the periods (in terms of k) of the components are approximately 7 and 3 for models with $X_c = 0.5$ and 0.3. Following equation (14), these periods should correspond to a location of the discontinuity (expressed as $\Pi_0/\Pi_\mu \simeq k^{-1}$) of 0.14 and 0.3: as shown in Fig. 7, these estimates very accurately describe the locations of the sharp variation of N in the models.

Numerical solutions of equation (26), found using a bracketing-bisection method (see Press et al. 1992), are shown in Fig. 8. As is clearly visible when comparing Figs 8 and 4, we find that the solutions of equation (26) better match the oscillatory behaviour of the period spacing than the sinusoids of equation (13).

In the following section, we extend to a wider range of main-sequence models the analysis presented for a $6\,M_\odot$ model.

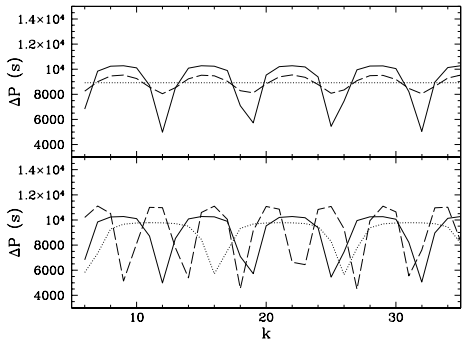

Figure 8. Period spacing $\Delta P = P_{k+1} - P_k$ calculated from numerical solutions of equation (26). All solutions are calculated for $\ell = 1$ modes and $\Pi_0 = 639$ s. In the upper panel, we fix the value of Π_0/Π_μ to 0.15 and vary α: $\alpha = 0.35$ (continuous line), $\alpha = 0.75$ (dashed line) and $\alpha = 1$ (dotted line). In the lower panel, we fix the value of α to 0.35 and vary the value of Π_0/Π_μ: $\Pi_0/\Pi_\mu = 0.15$ (continuous line), 0.225 (dashed line) and 0.1 (dotted line).

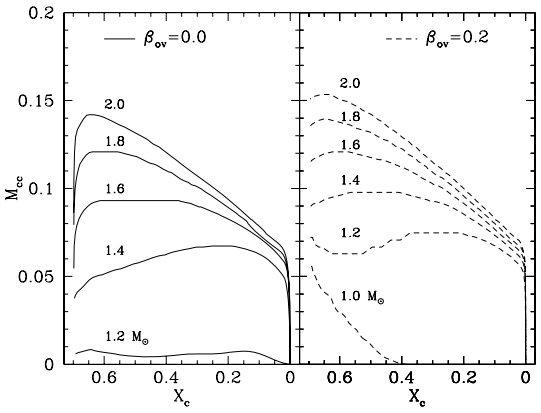

Figure 9. Fractional mass of the convective core as a function of central hydrogen abundance for models computed with (right-hand panel) and without (left-hand panel) overshooting, for masses between 1.0 and 2 $M_\odot$. β is the overshooting parameter as defined in Section 4.2.1.

4 APPLICATION TO STELLAR MODELS

The occurrence of a sharp chemical composition gradient in the central region of a star is determined by the appearance of convection in the core and by the displacement of the convective core boundary during the main sequence. For a given chemical composition, and if no non-standard transport process is included in the modelling, the transition from radiative to convective energy transport, as well as the shape of the μ gradients in the central stellar region, is determined by the mass of the model. On the other hand, additional mixing processes may alter the evolution of the convective core and the detailed properties of the chemical composition profile.

As shown in the previous section, the features of periodic signals in the period spacing of high-order g modes can provide very important information on the size of the convective core and on the mixing processes able to change the μ gradients generated during the evolution.

In this section, we present a survey of the properties of adiabatic $\ell = 1$ high-order g modes in main-sequence stars with masses from 1 to 10 $M_\odot$, and for four different evolutionary stages: those corresponding to a central hydrogen mass fraction X_c of 0.7, 0.5, 0.3 and 0.1. All these models were computed with the same initial chemical composition $(X_0, Z_0) = (0.70, 0.02)$. The adiabatic oscillation frequencies were computed with LOSC (Scuflaire et al. 2007a).

We first study how the properties of high-order gravity modes depend on the mass and the evolutionary stage of the model (Section 4.1). In a second step, we evaluate the effects of the inclusion of extra-mixing such as overshooting, diffusion and turbulent mixing (Section 4.2). The behaviour of modes with different ℓ will be briefly addressed in Section 4.3.

4.1 Convective core evolution: stellar mass dependence

In our analysis of the signatures of the μ gradients on g modes, we consider three stellar mass domains: (i) $M < M_{\rm Lcc}$, with $M_{\rm Lcc}$ being the minimum mass required to keep a convective core during the main sequence; (ii) $M_{\rm Lcc} \leqslant M \leqslant M_{\rm gc}$, for which the mass of the convective core increases during part of the main sequence and (iii) $M > M_{\rm gc}$ for which the convective core recedes as the star evolves. The situations described above are presented in Fig. 9, where the size in mass of the convective core is shown as a function of the central hydrogen abundance (and therefore of the age) of the star. The exact values of $M_{\rm Lcc}$ and $M > M_{\rm gc}$ depend on the chemical composition and, as we will see below, on extra-mixing processes.

4.1.1 Models with a radiative core

As a first example, we consider the evolution of the period spacing on the main sequence in models without a convective core, e.g. in a 1 $M_\odot$ star. The behaviour is substantially different from higher mass models: ΔP, as shown in Fig. 10, considerably decreases during the main sequence: this can easily be understood recalling the first-order asymptotic expression for the mean period spacing. The increase of N near the centre of the star, due to the mean molecular weight gradient developing in a radiative region (see upper panel of Fig. 10), has a larger and larger contribution to $\int \frac{N}{x'}\,{\rm d}x'$, leading to a significant reduction of the mean period spacing. The increase of N near the centre is, however, not sufficient to produce any periodic component of appreciable amplitude in the period spacing (see lower panel of Fig. 10).

4.1.2 Models with a growing convective core on the main sequence

In models with masses between $M_{\rm Lcc}$ and $M_{\rm gc}$, the contribution of nuclear burning through CNO cycle becomes more and more important as the star evolves on the main sequence (see e.g. Gabriel & Noels 1977; Crowe & Mitalas 1982; Popielski & Dziembowski 2005). The ratio L/m in the nuclear burning region becomes large enough to alter the behaviour of $\nabla_{\rm rad}$: the latter increases and so does the size of the convective core.

A growing convective core generates a discontinuity in the chemical composition at its boundary (see Fig. 11), and may lead to an inconsistency in the way the convective boundary is defined. The situation is illustrated in Fig. 12: the discontinuous hydrogen profile forces the radiative gradient to be discontinuous and to increase outside the region that is fully mixed by convection, and therefore, this region should be convective as well! If this is the case, then we have a contradictory situation: if we allow this region to have the same chemical composition as the core, then $\nabla_{\rm rad}$ decreases and the region becomes radiative again. The question of the semiconvection onset in models with masses in the range 1.1–1.6 was already addressed by Gabriel & Noels (1977) and Crowe & Mitalas (1982) quite some time ago. Nevertheless, what happens

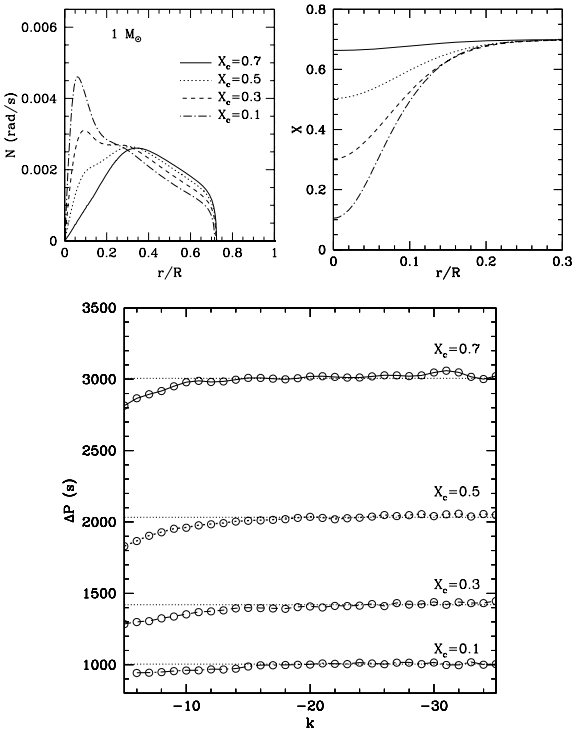

Figure 10. Upper left panel: N as a function of the normalized radius in $1\,M_\odot$ models with decreasing central hydrogen abundance. Upper right panel: hydrogen abundance profile versus r/R. Lower panel: g-modes period spacing as a function of the radial order k. The asymptotic value of ΔP (predicted by equation 4) is represented, for each model, by dotted lines.

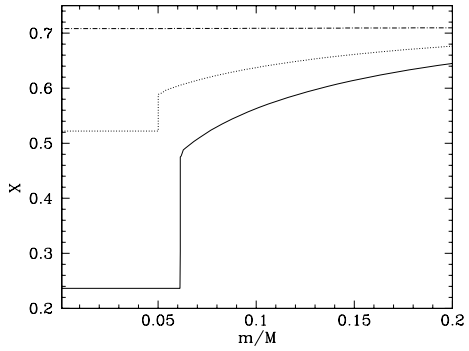

Figure 11. The discontinuous chemical composition profile generated by a growing convective core in $1.3\,M_\odot$ (see Fig. 12) when no extra-mixing outside the core is allowed.

in this so-called 'semi-convective' region is still a matter of debate. Some mixing is likely to take place, so that the composition gradients are adapted to obtain $\nabla_{\rm rad} = \nabla_{\rm ad}$ in the semiconvective region.

Even if no specific mixing is added in the semiconvective region, the μ gradient at the boundary of the convective core is very sensitive to the details of the numerical algorithm used in describing the core evolution. In fact, a strict discontinuity in chemical composition is only obtained if the border of the convective region is treated with a double mesh point (Fig. 11 for instance). This 'unphysical' framework leads to a problem when computing the Brunt–Väisälä frequency. The numerical difficulty can, however, be avoided keeping a quasi-discontinuous chemical composition, with a sharp change of X in an extremely narrow region ($\delta_0 = x_\mu - x_0$) outside the convective core (x_0). From equations (10) and (13), it is evident that the signal in the period spacing will then have an almost infinite period.

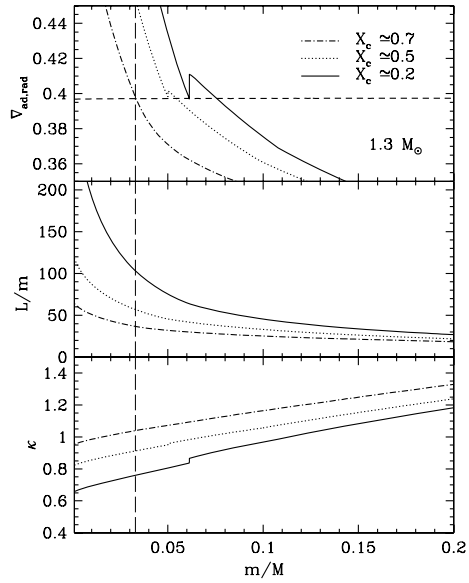

Figure 12. Upper panel: Radiative gradient in the inner regions of $1.3\,M_\odot$ models at different stages on the main sequence. The adiabatic gradient is represented with a short-dashed line. Middle panel: ratio $L(r)/m(r)$. During the evolution, the large increase of L/m at the former border of the convective core dominates the behaviour of $\nabla_{\rm rad}$. The vertical dashed line denotes the border of the convective core in the ZAMS model. Lower panel: behaviour of κ for the same models as in the other panels.

Of course, any treatment of the semiconvective region should destroy the discontinuity leading to a wider μ-gradient region. The chemical composition discontinuity may also be removed by a sort of 'numerical diffusion' that appears when the grid of mesh points (necessarily finite) in the modelling does not follow the convection limits. That is the case of the evolution code (CLES; Scuflaire et al. 2007b) used to compute most of the stellar models presented in this paper. In these models, the region where the discontinuity would be located is assumed to have an intermediate chemical composition between the one in the outermost point of the convective core and the one in the innermost point of the radiative region. The final effect is to have a partial mixing at the edge of the convective core, and thus to remove the discontinuity in μ.

Furthermore, in models with a mass $M \simeq M_{\rm Lcc}$, e.g. $M = 1.2\,M_\odot$, the convective core is so small ($m/M \sim 0.01$) that the period spacing resembles the behaviour of the $1\,M_\odot$ model. We note, however, the appearance of oscillatory components in ΔP in the model with $X_{\rm c} \simeq 0.1$ (see Fig. 13). The sharp variation of N located at $\Pi_0/\Pi_{\rm r} \simeq 0.1$ is large enough to generate components with a periodicity of $10\,k$ in ΔP. In more massive models, the μ gradient becomes larger and so does the amplitude of the components in the period spacing (see e.g. Fig. 14).

4.1.3 Models with a receding convective core

In models with shrinking convective cores, the situation is much simpler. If $M > M_{\rm gc}$, the dominant term in the behaviour of the radiative gradient is the opacity and, since $\kappa \propto (1 + X)$, $\nabla_{\rm rad}$ decreases with time as X decreases: the boundary of the convective core is displaced towards the centre. A receding convective core leaves behind a chemical composition gradient that is responsible

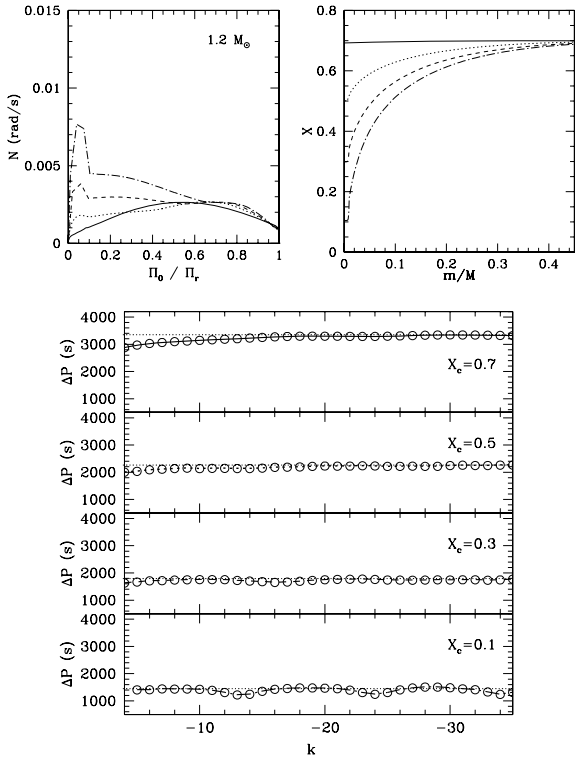

Figure 13. Behaviour of the Brunt–Väisälä frequency (upper left panel), of the hydrogen abundance profile (upper right panel) and of the $\ell = 1$ g-mode period spacing in models of $1.2\,M_\odot$. We consider, as in all the following figures, several models on the main sequence with decreasing central hydrogen abundance (X_c 0.7, 0.5, 0.3 and 0.1).

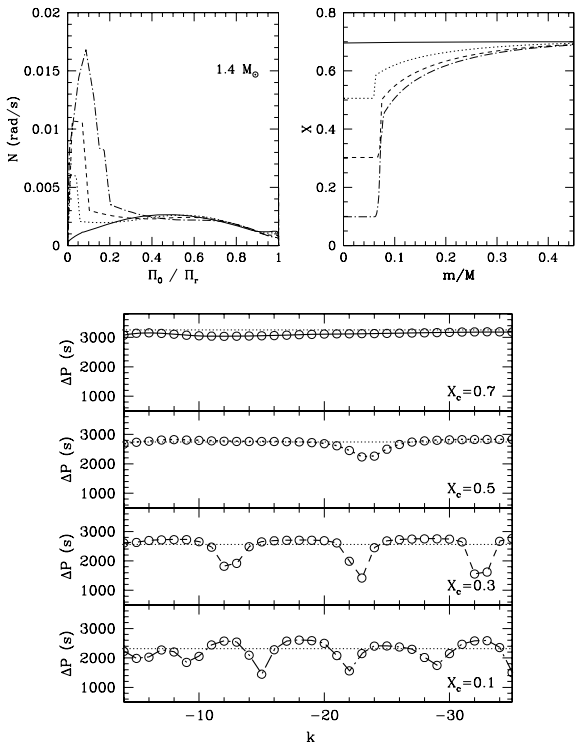

Figure 14. Same as Fig. 13 for $1.4\,M_\odot$ models.

for an abrupt change in the N profile (as in Fig. 1). Such a sharp feature which is a direct consequence of the evolution of a convective core leaves a clear signature in the periods of gravity modes.

That behaviour is shown in Figs 15 and 16 for models of 1.6 and $6\,M_\odot$ (for larger masses, the behaviour is almost identical to that of $6\,M_\odot$). The periodicity of the components in ΔP can be easily related to the profile of the Brunt–Väisälä frequency by means of expression (14). For instance, the $\Delta k = 7$ in Fig. 16 (lower panel, $X_c = 0.50$) corresponds to the sharp signal in N at $\Pi_0/\Pi_r \sim 0.14$. As the star evolves, the sharp feature in N is shifted to higher Π_0/Π_r, and when $\Pi_0/\Pi_\mu \simeq 0.5$ a kind of beating occurs in the period spacing due to the fact that the sampling frequency is about half the frequency of the periodic component.

The amplitude of the variation of ΔP as a function of the mode order is well reproduced by equation (26) (compare e.g. Figs 16 and 8), but not by equation (13) that predicts a sinusoidal behaviour. However, having a simple analytical relation between the amplitude of the components and the sharpness of $\delta N/N$ is not straightforward from equation (26).

It can also be noted that oscillatory components of small amplitude occur already in zero-age main-sequence stars with $M \gtrsim 6\,M_\odot$ (see e.g. Fig. 16, solid lines). Although a chemical composition gradient is not yet present in these models, the bump in the Brunt–Väisälä frequency due to an increase of the opacity[2] at a temperature of $\sim 3 \times 10^6$ K ($\Pi_0/\Pi_r \simeq 0.8$) is able to produce such a deviation from constant ΔP. It is not surprising that the effects of a sharp feature located near the surface can mimic the effect of a perturbation in the core: as shown by Montgomery et al. (2003) the signature in high-order g modes of a perturbation in N located at a normalized buoyancy radius $r_{BV} = \Pi_0/\Pi_r$ is aliased to a signal whose source is located at $1 - r_{BV}$. The signal shown in Fig. 16 could indicate a source at $0.2\ \Pi_0/\Pi_r$ which is in fact

[2] Mainly due to C, O, Ne and Fe transitions (see e.g. Rogers & Iglesias 1992; Seaton & Badnell 2004).

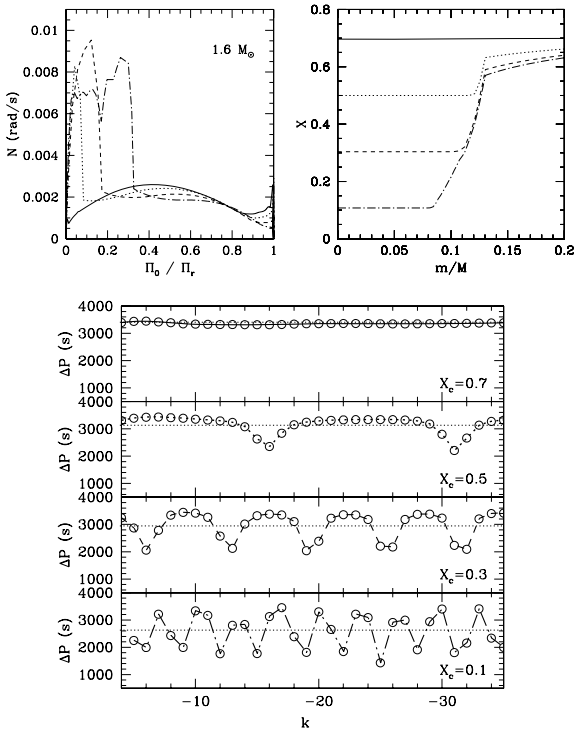

Figure 15. Same as Fig. 13 for $1.6\,M_\odot$ models.

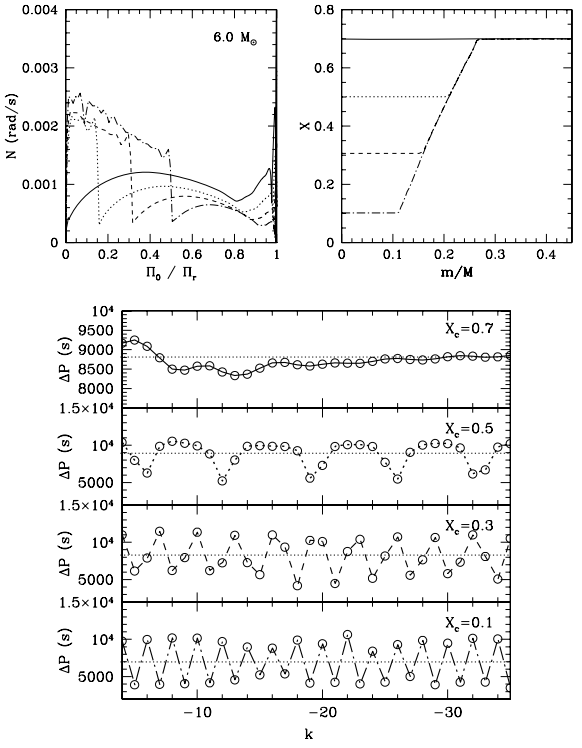

Figure 16. Same as Fig. 13 for 6.0 $M_\odot$ models. In the homogeneous ZAMS model ($X_c \simeq 0.7$, full lines), a sharp variation in N located at $\Pi_0/\Pi_r \simeq 0.8$ generates a periodic signal of small amplitude in the period spacing. Note that for this model, to make such a component more visible in ΔP, the y-axis scale has been modified.

approximatively an alias $(1 - 0.2)$ of the source at $0.8\ \Pi_0/\Pi_r$. The amplitude of this signal increases with the stellar mass as the contribution of this opacity bump becomes dominant in the behaviour of ∇_{rad} (and therefore of N). In fact, for large enough stellar masses, a convective shell can appear at a temperature $\sim 3 \times 10^6$ K. The amplitude of such components is, however, less than 1000 s and therefore much smaller than the amplitude due to the chemical composition gradient at the edge of the convective core.

The g-mode period spacing is clearly different depending on the mass and age of the models. While in models without (or with a very small) convective core the mean value of the period spacing decreases with age (see Section 4.1.1), for more massive models the period spacing does not significantly change with age. In stars with larger convective cores, the chemical composition gradient is located at a larger fractional radius, giving a smaller contribution to $\int \frac{N}{x'}\,dx'$, and thus to ΔP, as predicted from the asymptotic expression. In these models, the age effect is made evident, however, through the appearance of the periodic signal in the period spacing, whose periodicity is directly linked to the chemical gradient left by the evolution of the convective core.

4.2 Effects of extra-mixing

The comparison between theoretical models and observations clearly shows that the standard stellar modelling underestimates the size of the central mixed region (see e.g. Andersen, Clausen & Nordstrom 1990; Ribas, Jordi & Giménez 2000). This fact is generally accepted, but there is no consensus about the physical processes responsible for the required extra-mixing that is missing in the standard evolution models: overshooting (e.g. Schaller et al. 1992), microscopic diffusion (Michaud et al. 2004), rotationally induced mixing (see e.g. Maeder & Meynet 2000; Mathis, Palacios & Zahn 2004, and references therein) or mixing generated by propagation of internal waves (e.g. Young & Arnett 2005). The shape of the composition transition zone is a matter of great importance as far as asteroseismology is concerned. In particular, it significantly affects the term ∇_μ appearing in the Brunt–Väisälä frequency and plays a critical role in the phenomenon of mode trapping.

It is therefore evident that the size and evolution of the convective core, as well as the μ gradients that it generates, can be strongly affected by the occurrence of mixing processes. In the following paragraphs, we study how these effects are reflected on the high-order g modes. We have computed models with overshooting, microscopic diffusion, turbulent mixing, and we have compared their adiabatic g-mode periods with those derived for models computed without mixing and with the same central hydrogen abundance.

4.2.1 Overshooting

Penetration of motions beyond the boundary of convective zones defined by the Schwarzschild stability criterion has been the subject of many studies in an astrophysical context (see e.g. Zahn 1991). Unfortunately, features such as extension, temperature gradient and efficiency of the mixing in the overshooting region cannot be derived from the local model of convection currently used in stellar evolution computations. As a consequence, this region is usually described in a parametric way. In the models considered here, the thickness of the overshooting layer *ov* is parametrized in terms of the local pressure scaleheight H_p: $ov = \beta \times (\min(r_{cv}, H_p(r_{cv})))$ (where r_{cv} is the radius of the convective core and β is a free parameter). We assume instantaneous mixing both in convective and in overshooting regions. The temperature gradient in the overshooting region is left unchanged (i.e. $\nabla = \nabla_{rad}$). Therefore, overshooting simply extends the region assumed to be fully mixed by convection. The larger hydrogen reservoir, due to an increase of the mixed region, translates into a longer core-hydrogen burning phase.

The adopted amount of overshooting also determines the lowest stellar mass where a convective core appears. For sufficiently large values of β, the convective core that develops in the pre-main-sequence phase persists during the main sequence in models with $M < M_{Lcc}$ (as in Fig. 9). In these models, the convective core is maintained thanks to the continuous supply of ^{3}He that sustains the highly temperature-dependent nuclear reaction $^3\mathrm{He} + {}^3\mathrm{He} \rightarrow {}^4\mathrm{He} + 1\mathrm{H} + {}^1\mathrm{H}$, keeping the proton–proton chain in an out-of-equilibrium regime. The inclusion of overshooting changes the value of the mass corresponding to the transition between models with a convective core that grows/shrinks during the main sequence (Fig. 9, right-hand panel). Finally, the effect of overshooting on the μ gradients depends on whether the nuclear reactions occur only inside the convective core or also outside. In Fig. 17, we present the chemical composition profile, the behaviour of N and of the period spacing, in models computed with overshooting ($\beta = 0.2$). These models have a larger fully mixed region than those computed without overshooting. The chemical composition gradient is then displaced to a higher mass fraction. If we compare with models of similar central hydrogen abundance, however, this does not necessarily imply that the sharp feature in N is located at a different normalized buoyancy radius (Π_0/Π_μ).

(i) In 6 $M_\odot$ models (right-hand column in Fig. 17), for instance, neither the sharpness of the abrupt variation in N nor its location in terms of Π_μ changes when comparing models computed with and without overshooting.

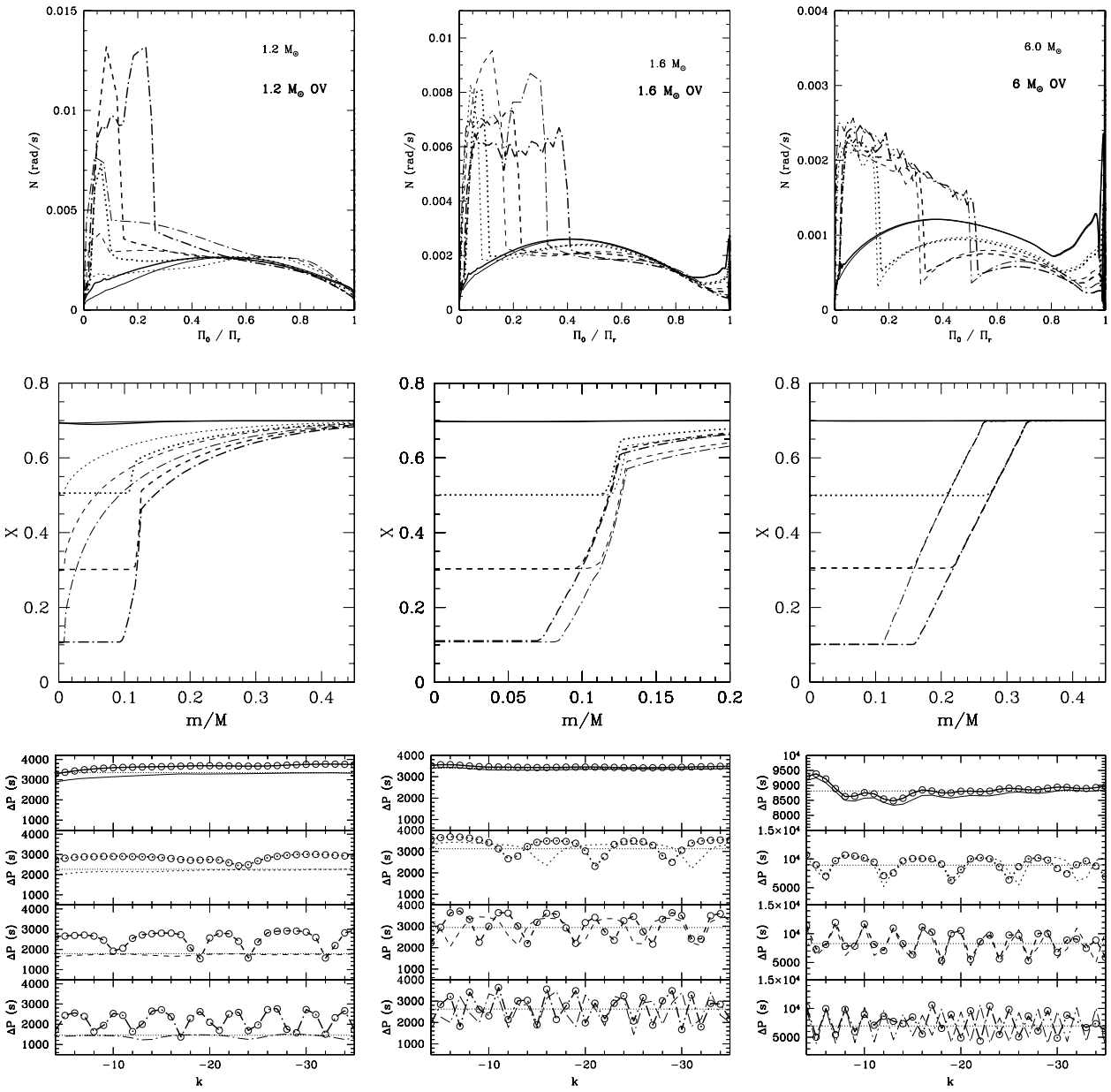

Figure 17. Behaviour of the Brunt–Väisälä frequency (upper row), of the hydrogen abundance profile (central row) and of the $\ell = 1$ g-mode period spacing (lower row) in models of 1.2, 1.6 and 6 $M_\odot$ computed with (thick lines) or without (thin lines) overshooting.

(ii) The situation changes in lower mass models, for example, in 1.6 $M_\odot$ models (central column in Fig. 17). Here, the periodicity of the components in ΔP differs if we include overshooting or not. A change in not only the location, but also in the value of the μ gradient (as nuclear reactions take place outside the core as well), is responsible for a different behaviour of the oscillatory components in ΔP.

(iii) In models with a mass $M \simeq M_{\rm Lcc}$, e.g. $M = 1.2\,M_\odot$, the inclusion of overshooting dramatically increases the size of the fully mixed region. The oscillatory components in ΔP have different periods and much larger amplitudes than in the case of models without overshooting (see left-hand column of Fig. 17).

As we mentioned above, not only the extension of the overshooting region, but also its temperature stratification is uncertain. However, the effect on ΔP of considering convective penetration ($\nabla =$ $\nabla_{\rm ad}$ in the 'extended' convective core) instead of simple overshooting is found to be small (see Straka, Demarque & Guenther 2005; Godart 2007).

4.2.2 Effects of microscopic diffusion

Other physical processes, different from overshooting, can lead to an increase of the central mixed region or modify the chemical composition profile near the core.

Michaud et al. (2004) and Richard (2005) have shown that microscopic diffusion can induce an increase of the convective core mass for a narrow range of masses, from 1.1 to 1.5 $M_\odot$, and that the effect decreases rapidly with increasing stellar mass. In this mass range, as previously described, the mass of the convective core increases during the MS evolution instead of decreasing, as it occurs for larger masses. As a consequence, a sharp gradient of chemical

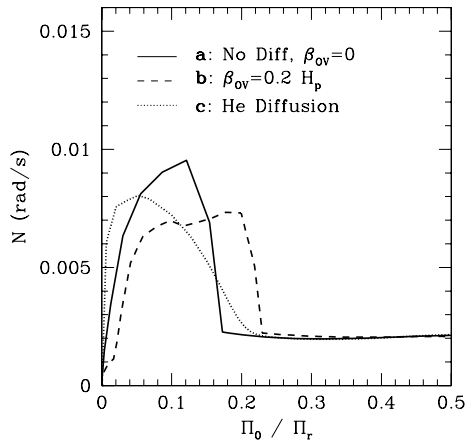

Figure 18. Behaviour of the Brunt–Väisälä frequency in models of $1.6\,M_\odot$ with $X_c \simeq 0.3$. The different lines correspond to models calculated with no extra-mixing (continuous lines), overshooting (dashed) and helium diffusion (dotted). The different location and sharpness of the chemical composition profile determine the behaviour of N.

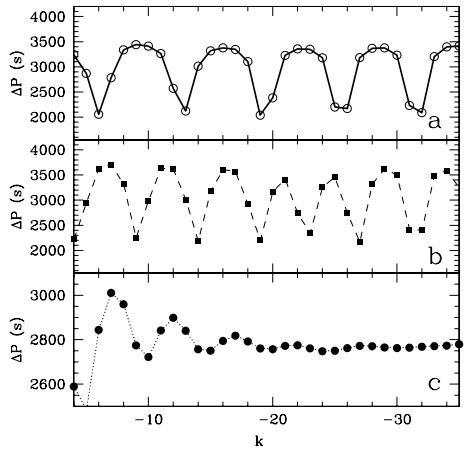

Figure 19. Period spacing of $\ell = 1$ g modes as a function of the radial order k for the $1.6\,M_\odot$ models presented in Fig. 18.

composition appears at the border of the convective core, making the diffusion process much more efficient in that region.

Fig. 18 shows the effect of including gravitational settling, thermal and chemical diffusion of hydrogen and helium in a $1.6\,M_\odot$ model. If only He and H diffusion is considered in the modelling, we find that a smoother chemical composition profile is built up at the edge of the convective core (see Fig. 18) preventing the presence of a discontinuity in μ caused by a growing convective core. Comparing models calculated with or without diffusion, the location of the convective core boundary is not significantly changed. Nevertheless, a less sharp variation in the Brunt–Väisälä frequency is responsible for a considerable reduction of the amplitude of the components in the period spacing (see Fig. 19). It was in fact predicted in Section 3.1 that a discontinuity not in N itself, but in its first derivative, would generate a periodic component whose amplitude decreases with the period: this simplified approach is therefore sufficient to account for the behaviour of ΔP in models with a smoother chemical composition gradient (see equation 16).

When diffusion of Z is also included, the overall effect of diffusion is no longer able to erode the sharp chemical composition gradient and to prevent the formation of a semiconvective zone, on the contrary, diffusion of Z outside the core makes the occurrence of semiconvection easier (see also Richard, Michaud & Richer 2001; Michaud et al. 2004; Montalbán, Théado & Lebreton 2007). If chemical diffusion is accountable for a smoother chemical composition profile in intermediate- and low-mass stars, we find that such an effect disappears as higher masses are considered and evolutionary time-scales decrease. In fact, we find that in models with $M \gtrsim 4\,M_\odot$ diffusion has no effect either on the Brunt–Väisälä frequency profile near the hydrogen burning core, or on the behaviour of the period spacing.

As higher masses are considered, the effect of microscopic diffusion on the stellar structure near the core becomes negligible but, other mixing processes can partly erode the chemical composition gradients.

4.2.3 Rotationally induced mixing

Rotationally induced mixing can influence the internal distribution of μ near the energy generating core. Different approaches have been proposed to treat the effects of rotation on the transport of angular momentum and chemicals (see e.g. Heger & Langer 2000; Maeder & Meynet 2000; Pinsonneault et al. 1989, and references therein). Such an additional mixing has an effect on the evolutionary tracks which is quite similar to that of overshooting, but it leads also to a smoother chemical composition profile at the edge of the convective core.

Since our stellar evolution code does not include a consistent treatment of rotational effects, we simply include the chemical turbulent mixing by adding a turbulent diffusion coefficient (D_T) in the diffusion equation. In our parametric approach, D_T is assumed to be constant inside the star and independent of age.

The simplified parametric treatment of rotationally induced mixing used in this work has the aim of showing that if an extra-mixing process, different from overshooting, is acting near the core it will produce a different chemical composition profile in the central regions of the star and leave a different signature in the periods of gravity modes. The effects of such a mixing on the evolutionary tracks (see Fig. 20) and on the internal structure clearly depend on the value of D_T.

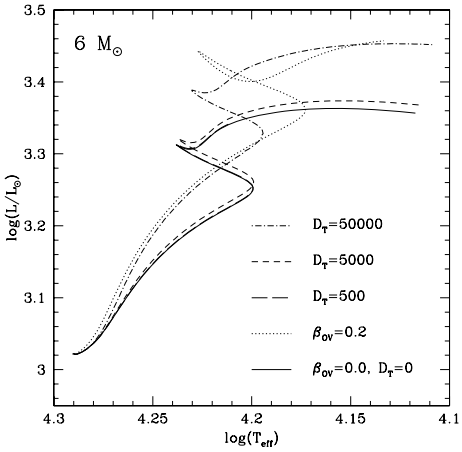

Figure 20. HR diagram showing evolutionary tracks of $6\,M_\odot$ models calculated with different extra-mixing processes. The evolutionary track computed with $D_T = 500$ is superposed to that without extra-mixing (continuous line).

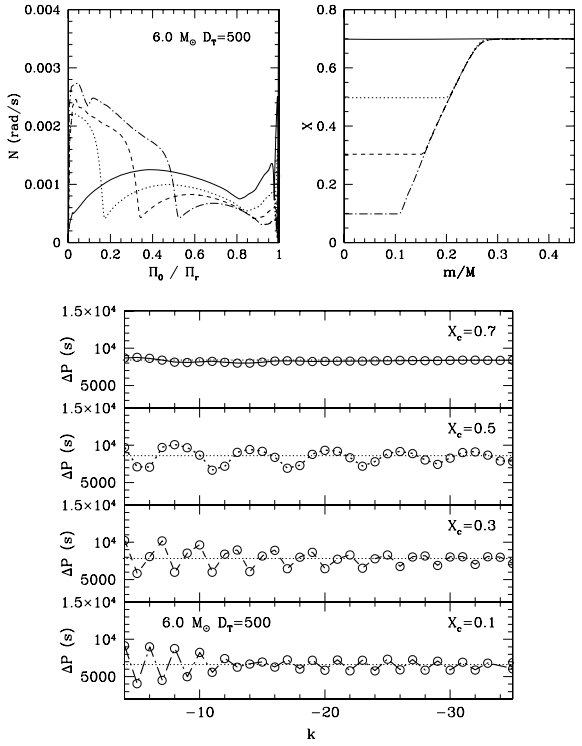

Figure 21. Behaviour of the Brunt–Väisälä frequency (upper left panel), of the hydrogen abundance profile (upper right panel) and of the $\ell = 1$ g-mode period spacing in models of $6.0\,M_\odot$ computed with a turbulent diffusion coefficient $D_T = 500$.

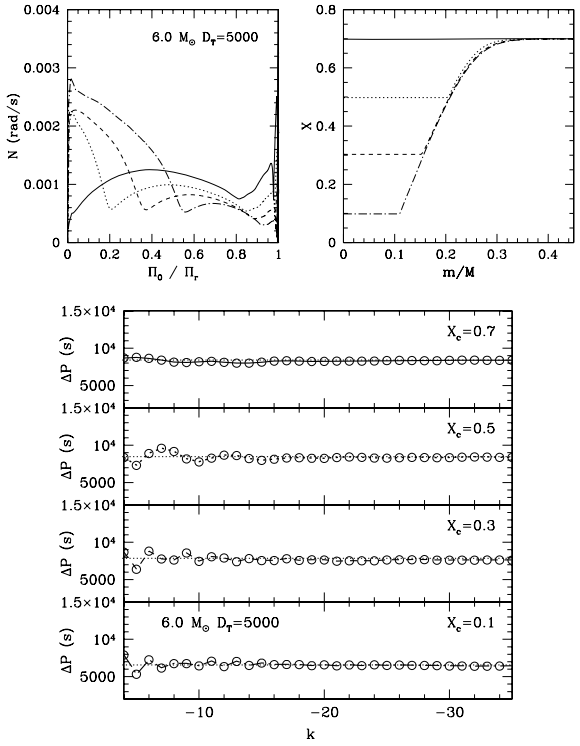

Figure 22. As in Fig. 22 but for models with $D_T = 5000$.

As an example, we consider models of a $6\,M_\odot$ star computed with three different values of the turbulent-diffusion coefficient $D_T = 5 \times 10^2, 5 \times 10^3$ and 5×10^4 cm^2 s^{-1}. The lowest D_T value provides an evolutionary track that overlaps the one computed with no mixing; however, its effect on the chemical composition gradient (see Fig. 21) is sufficient to affect ΔP for high-order modes. In order to significantly change the periods of low-order modes, a much more effective mixing is needed. The value $D_T = 5 \times 10^3$ leads to a slightly more luminous evolutionary track, but such a mixing has a substantial effect on the period spacing: the amplitude of the periodic components in ΔP becomes a decreasing function of the radial order k (see Figs 21 and 22). As in the case of helium diffusion (see Section 4.2.2), this behaviour can be easily explained by the analytical approximation presented in Section 3.1 (equation 16), provided the sharp feature in N is modelled not as a step function but, for instance, as a ramp (equation 15).

If a significantly more effective mixing is considered (e.g. $D_T = 50\,000$; see Figs 20 and 23), the corresponding evolutionary track is close to that obtained by including a classical overshooting but the periodic components in ΔP are no longer present.

The effects of such a turbulent mixing on low-order gravity modes and avoided crossings will be addressed in detail in a future work.

In order to check that our parametric approach is at least in qualitative agreement with the outcome of models where rotationally induced mixing is treated consistently, we present for comparison a sequence of models computed with the Geneva evolutionary code (Meynet & Maeder 2000; Eggenberger et al. 2007). We considered a $6\,M_\odot$ model with an initial surface rotational velocity of 25 km s^{-1}, the typical $v \sin i$ for SPBs stars (Briquet et al. 2007). As the model evolves on the MS, the effects on the HR diagram (Fig. 24) and on the chemical composition gradient in the core (Fig. 25) are very similar to those of the model computed with a uniform turbulent diffusion coefficient $D_T = 5 \times 10^3$. This is not surprising since, in the central regions, the total turbulent diffusion coefficient shown

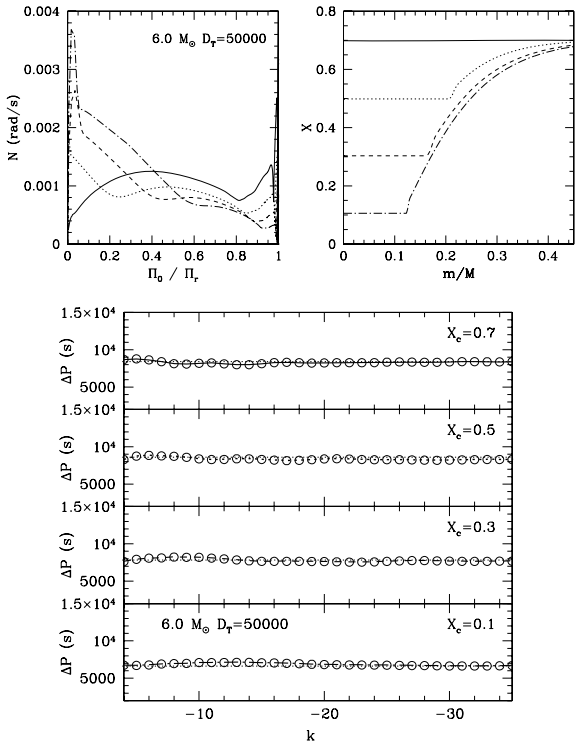

Figure 23. As in Fig. 22 but for models with $D_T = 50000$. The effect of such a mixing on the evolutionary track is shown in Fig. 20.

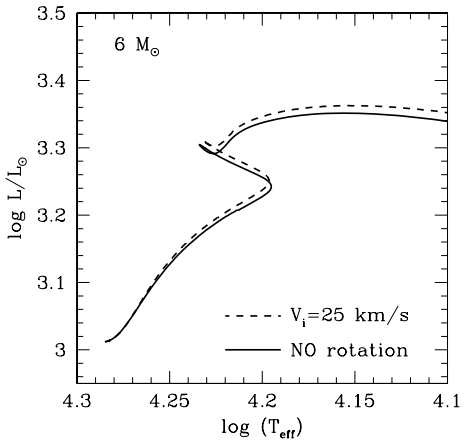

Figure 24. HR diagram showing evolutionary tracks of $6\,M_\odot$ models calculated with the Geneva evolutionary code. The full line evolutionary track is computed without rotation, whereas in the models evolving on the dotted track an initial surface velocity of 25 km s^{-1} is assumed.

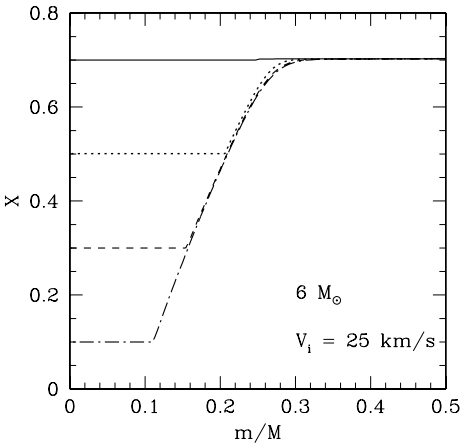

Figure 25. Hydrogen abundance in the core of $6\,M_\odot$ models with an initial surface velocity of 25 km s^{-1}.

in Fig. 26 does not change considerably in time and its magnitude is of the order of a few thousands cm^2 s^{-1}.

4.3 Modes of different degree and low radial order

In the previous sections, we analysed the properties of ΔP for $\ell = 1$, high-order g modes. Does the period spacing computed with modes of different degree ℓ, or with low radial order k, have a similar behaviour? In Fig. 27, we consider the period spacing computed with $\ell = 2$ periods $P_{k,\ell=2}$ scaled by the ℓ-dependent factor suggested by equation (4), i.e. $P'_{k,\ell=2} = \sqrt{3}\ P_{k,\ell=2}$. Except for the oscillation modes with the lowest radial orders, we note in Fig. 27 that the period spacing of modes of degree $\ell = 1$ and 2 has the same behaviour, provided that the dependence on ℓ given by equation (4) is removed.

Though the asymptotic approximation is valid for high-order modes, we see in Fig. 27 (as well as in the figures presented in the previous sections) that the description of the period spacing as the superposition of the constant term derived from equation (4) and periodic components related to ∇_μ is able to accurately describe the periods of gravity modes even for low-order k. This suggest that, at least qualitatively, the description of g modes presented in this work could represent a useful tool to interpret the behaviour of low-order

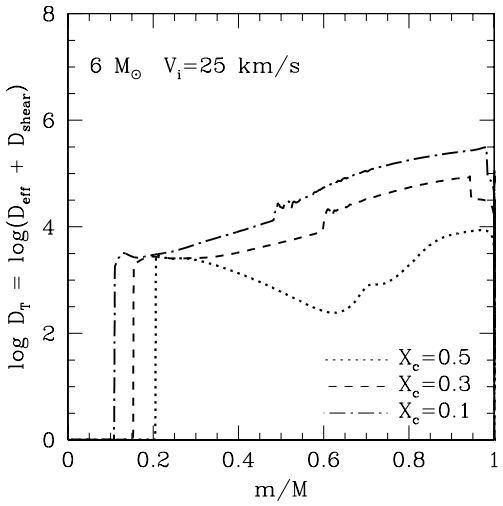

Figure 26. Total diffusion coefficient $D_{\rm T}$ as a function of the normalized mass in $6\,M_\odot$ models evolving on the main sequence. The initial surface velocity assumed is 25 km s^{-1} . $D_{\rm T}$ includes both the effects of shear ($D_{\rm shear}$) and meridional circulation ($D_{\rm eff}$).

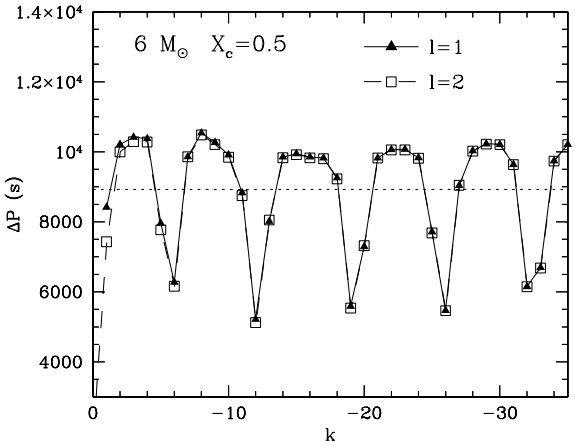

Figure 27. Period spacing for $6\,M_\odot$ models with $X_{\rm c} = 0.5$. The period spacing computed with $\ell = 2$ modes is multiplied by $\sqrt{3}$, as suggested by equation (4).

g modes observed in other classes of pulsators, such as β Cephei and δ Scuti stars. This subject will be addressed in a second paper.

5 CHALLENGES FOR ASTEROSEISMOLOGY

Asteroseismology of high-order g-mode main-sequence pulsators is not an easy task. The long oscillation periods and the dense frequency spectrum in these stars require long and continuous observations in order to resolve single oscillation frequencies. As already stated clearly in Dziembowski et al. (1993), observations of at least 70 days are needed to resolve the period spacing in a typical SPB star. In addition to large observational efforts that have been made from the ground (see e.g. De Cat & Aerts 2002; De Cat et al. 2007 for SPB stars and Mathias et al. 2004; Henry, Fekel & Henry 2007 for γ Dor), long, uninterrupted space-based photometric time series will soon be provided by CoRoT. In order to estimate if the CoRoT 150 d-long observations have a frequency resolution sufficient to resolve the period spacing of a typical SPB star, we simulated a time series of $\ell = 1$ and 2 high-order g modes that are expected to be

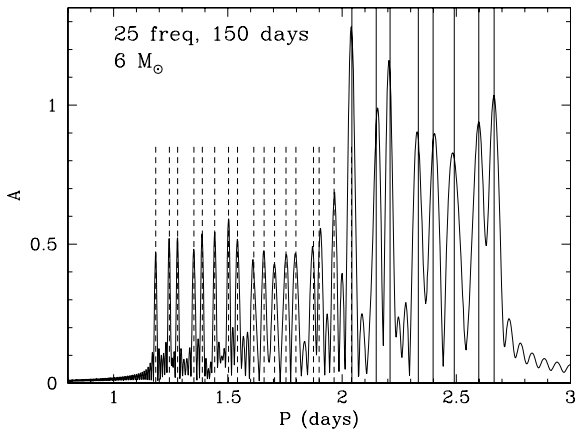

Figure 28. Power spectrum of simulated time series for a $6\,M_{\odot}$ model. The vertical solid and dashed lines represent the input oscillation frequencies of, respectively, $\ell = 1$ and 2 modes.

excited in a $6\,M_{\odot}$ star with $X_c = 0.2$ computed without overshooting. The excitation of oscillation modes has been computed using the non-adiabatic code MAD (Dupret et al. 2003). Random initial phases have been considered in the sine curves describing the 25 frequencies included in the simulations, and amplitudes of 1 and 0.5 (on an arbitrary scale) have been assumed for $\ell = 1$ and 2 modes, respectively. The generated time series has been analysed using the package PERIOD04 (Lenz & Breger 2005). As it is shown in the resulting power spectrum (see Fig. 28), for such long observational runs (150 d) the input frequencies can be accurately recovered even for the largest periods of oscillation. Thanks to the high-frequency resolution, the departures from a constant period spacing are also evident in the power spectrum.

We then simulate a time series for an additional $6\,M_{\odot}$ model that, despite having the same surface properties ($\log(L/L_{\odot}) = 3.21, \log(T_{\rm eff}) = 4.22$) as the previous one, is computed with turbulent diffusion ($D_T = 5000$). In this case, the power spectrum (see Fig. 29) shows a regular period spacing that, on the basis of the high-frequency resolution, can be easily distinguished from the one described in Fig. 28.

Even though frequency resolution may no longer be an issue in the very near future, there is a second well-known factor limiting asteroseismology of SPB and γ Dor stars: the effects of rotation on the oscillation frequency can severely complicate the high-order g-mode spectra. Referring once more to the work by Dziembowski et al. (1993), a first requirement in order to treat rotational effects as perturbations on the oscillation frequencies is the angular rotational velocity being sufficiently smaller than the oscillation frequency ($v_{\rm rot} \ll 2\pi R/P$, where R is the radius of the star and P the oscillation period). In the case of the models of an SPB star considered previously in this section, this translates into $v_{\rm rot} \ll 100\,{\rm km\,s^{-1}}$ considering the modes of longest period: this is significantly larger than the average vsini ($\sim$25 km s^{-1}) measured in SPB stars (see e.g. Briquet et al. 2007). In the case of γ Dor stars (see e.g. Suárez et al. 2005), a similar estimate limits the validity of the perturbative approach to rotational velocities of $\sim$50–70 km s^{-1}: for faster rotators non-perturbative approaches are needed (see Dintrans & Rieutord 2000; Rieutord & Dintrans 2002).

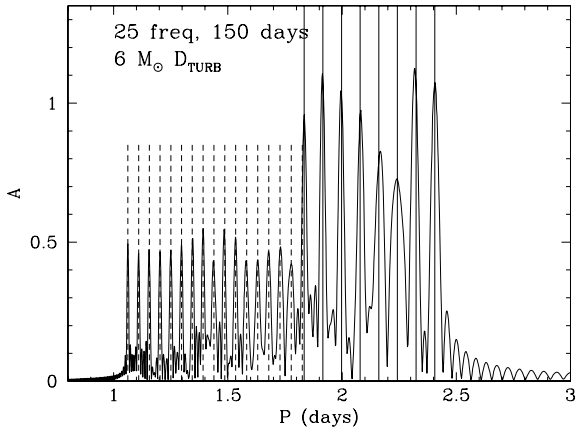

Figure 29. Same as Fig. 28 for a $6\,M_{\odot}$ model computed with turbulent diffusion in the core.

Even in the case of slow rotators, however, the rotational splittings may become as large as the period spacing itself. Such a large effect of rotation on the frequency spectrum can severely complicate the identification of the azimuthal order m and the degree ℓ of the observed modes. In fact, a simple mode identification based on the regular pattern expected from high-order g modes becomes inapplicable if the rotational splitting is of the same order as ΔP (see e.g. fig. 13 in Dziembowski et al. 1993). The identification of the modes would then need to be provided by photometric and spectroscopic mode identification techniques (see e.g. Balona 1986; Garrido, Garcia-Lobo & Rodriguez 1990; Aerts, de Pauw & Waelkens 1992; Mantegazza 2000; Briquet & Aerts 2003; Dupret et al. 2003; Zima 2006).

6 SUMMARY AND CONCLUSIONS

In this work, we investigated in detail the properties of high-order gravity in models of main-sequence stars. The chemical composition gradient that develops near the outer edge of the convective core leads to a sharp variation of the Brunt–Väisälä frequency. As we presented in Section 2, the latter is responsible for a periodic trapping of gravity modes in the region of chemical composition gradient, and it directly affects the period spacing of g modes.

In analogy with the works on white dwarfs by Brassard et al. (1992) and Montgomery et al. (2003), we show that in the case of main-sequence stars analytical approximations can be used to directly relate the deviations from a uniform period spacing to the detailed properties of the μ-gradient region that develops near the energy generating core. We find that a simple approximation of g-mode periods, based on the variational principle of stellar oscillations, is sufficient to explain the appearance of sinusoidal components in the period spacing. This approximation (see Section 3.1) relates the periodicity of the components to the normalized buoyancy radius of the glitch in N, and the amplitude of the components to the sharpness of the feature in N. In particular, if the sharp variation in N is modelled as a step function, the amplitude of such components is expected to be independent of the order of the mode k; whereas if the glitch in N is described with a ramp, the amplitude of the components decreases with k. A more accurate semi-analytical approximation of the period spacing, which considers the effects of the sharp feature in N on the eigenfunctions, is also given in Section 3.2.

We then presented a survey of the properties of high-order g modes in main-sequence models of masses between 1 and $10\,M_{\odot}$ (see Section 4). As a general result we found that, in models with a convective core, the period spacing of high-order g modes is accurately described by oscillatory components of constant amplitude, superposed to the mean period spacing predicted by the asymptotic

theory of Tassoul (1980). In Section 4.1, we showed that the period spacing depends primarily on the extension and behaviour of the convective core during the main sequence and, therefore, on the mass of the star.

In models without a convective core (see Section 4.1.1), the mean ΔP considerably decreases during the MS, whereas no significant deviation from a constant period spacing is present. For an intermediate range of masses (see Section 4.1.2), the convective core grows during most of the MS, generating an 'unphysical' discontinuity in μ if no mixing is added in the small semiconvective region that develops. We find that the behaviour of ΔP, and in particular the appearance of periodic components, depends on the treatment of this region. It is interesting to note that γ Doradus stars are in the mass domain where models show a transition between growing to shrinking convective cores on the main sequence. Gravity modes could therefore represent a valuable observational test to discriminate between the different prescriptions used in stellar models (see e.g. Popielski & Dziembowski 2005) to introduce the required mixing at the boundary of the convective core. In models with higher masses, the convective core recedes during the main sequence (see Section 4.1.3): this leaves behind a μ gradient that generates clear periodic components in ΔP. We found that the analytical expression derived in Section 3.1 allows to accurately recover the location and sharpness of the μ gradient from the amplitude and periodicity of the components in ΔP. In this mass domain, though the average period spacing does not change substantially with the age, the periodicity of the components does, and it therefore represents an indicator of the evolutionary state of the star.

In Section 4.2, we showed that also extra-mixing processes can alter the behaviour of ΔP, since they affect the size and evolution of the convective core, as well as the sharpness of the μ gradient. We first compared models with the same X_c, but computed with and without overshooting (see Section 4.2.1). We found that in models with small convective cores, or where nuclear reactions also take place in the radiative region, the different size of the fully mixed region changes the periodicity of the components in ΔP. In Section 4.2.3, we described how chemical mixing can severely affect the amplitude of the periodic components in ΔP. In models where turbulent mixing induced by rotation is considered, the smoother μ profile near the core leads to a discontinuity not in N itself, but in its first derivative: as suggested by the analytical approximation in Section 3.1, this leads to periodic components in ΔP whose amplitude decreases with the order of the mode. In the case of SPB stars, in particular, we find that the mixing induced by the typical rotation rates observed (i.e. $\simeq$25 km s^{-1}) is sufficient to significantly alter the properties of the g-mode spectrum.

Finally in Section 5, we discussed the difficulties encountered in the asteroseismology of γ Doradus and SPB stars. Even though a frequency resolution sufficient to resolve closely spaced periods will be provided by the forthcoming space-based observations, an asteroseismic inference on the internal structure will only be possible for stars with very slow rotation rates, and with reliably identified pulsation modes. Once these conditions are reached, we will be able to access the wealth of information on internal mixing which, as shown in this work, is carried by the periods of high-order gravity modes in main-sequence objects.

ACKNOWLEDGMENTS

AM and JM acknowledge financial support from the Prodex-ESA Contract Prodex 8 COROT (C90199). PE is thankful to the Swiss National Science Foundation for support.

REFERENCES

Aerts C., de Pauw M., Waelkens C., 1992, A&A, 266, 294
Andersen J., Clausen J. V., Nordstrom B., 1990, ApJ, 363, L33
Baglin A., Michel E., Auvergne M., The COROT Team, 2006, in Fletcher K., ed., ESA SP-624, Proc. SOHO 18/GONG 2006/HELAS I, Beyond the Spherical Sun. ESA, Noordwijk, p. 34.1
Balona L. A., 1986, MNRAS, 219, 111
Basu S., Antia H. M., 1995, MNRAS, 276, 1402
Berthomieu G., Provost J., 1988, in Christensen-Dalsgaard J., Frandsen S., eds, Proc. IAU Symp. 123, Advances in Helio- and Asteroseismology. Reidel, Dordrecht, p. 121
Brassard P., Fontaine G., Wesemael F., Kawaler S. D., Tassoul M., 1991, ApJ, 367, 601
Brassard P., Fontaine G., Wesemael F., Hansen C. J., 1992, ApJS, 80, 369
Briquet M., Aerts C., 2003, A&A, 398, 687
Briquet M., Hubrig S., De Cat P., Aerts C., North P., Schöller M., 2007, A&A, 466, 269
Chapellier E., Le Contel D., Le Contel J. M., Mathias P., Valtier J.-C., 2006, A&A, 448, 697
Christensen-Dalsgaard J., Gough D. O., Thompson M. J., 1991, ApJ, 378, 413
Crowe R. A., Mitalas R., 1982, A&A, 108, 55
De Cat P., Aerts C., 2002, A&A, 393, 965
De Cat P. et al., 2007, A&A, 463, 243
Dintrans B., Rieutord M., 2000, A&A, 354, 86
Dupret M.-A., De Ridder J., De Cat P., Aerts C., Scuflaire R., Noels A., Thoul A., 2003, A&A, 398, 677
Dupret M.-A., Grigahcène A., Garrido R., Gabriel M., Scuflaire R., 2004, A&A, 414, L17
Dziembowski W. A., Moskalik P., Pamyatnykh A. A., 1993, MNRAS, 265, 588
Eggenberger P., Meynet G., Maeder A., Hirschi R., Charbonnel C., Talon S., Ekström S., 2007, Ap&SS, in press (doi:10.1007/s10509-007-9511-y)
Gabriel M., Noels A., 1977, A&A, 54, 631
Garrido R., Garcia-Lobo E., Rodriguez E., 1990, A&A, 234, 262
Godart M., 2007, Communications in Asteroseismology, 150, 185
Gough D. O., 1990, in Osaki Y., Shibahashi H., eds, Lecture Notes in Physics Vol. 367, Progress of Seismology of the Sun and Stars. Springer Verlag, Berlin, p. 283
Gough D., 1993, in Zahn J.-P., Zinn-Justin J., eds, Astrophysical Fluid Dynamics. Elsevier Science Publisher, Amsterdam, p. 399
Guzik J. A., Kaye A. B., Bradley P. A., Cox A. N., Neuforge C., 2000, ApJ, 542, L57
Handler G., 1999, MNRAS, 309, L19
Handler G. et al., 2006, MNRAS, 365, 327
Heger A., Langer N., 2000, ApJ, 544, 1016
Henry G. W., Fekel F. C., Henry S. M., 2007, AJ, 133, 1421
Houdek G., Gough D. O., 2007, MNRAS, 375, 861
Jerzykiewicz M., Handler G., Shobbrook R. R., Pigulski A., Medupe R., Mokgwetsi T., Tlhagwane P., Rodríguez E., 2005, MNRAS, 360, 619
Kawaler S. D., 1995, in Stobie R. S., Whitelock P. A., eds, ASP Conf. Ser. Vol. 83, Astrophysical Applications of Stellar Pulsation. Astron. Soc. Pac., San Francisco, p. 81
Lenz P., Breger M., 2005, Commun. Asteroseismol., 146, 53
Maeder A., Meynet G., 2000, ARA&A, 38, 143
Mantegazza L., 2000, in Breger M., Montgomery M., eds, ASP Conf. Ser. Vol. 210, Delta Scuti and Related Stars. Astron. Soc. Pac., San Francisco, p. 138
Mathias P. et al., 2004, A&A, 417, 189
Mathias P. et al., 2006, Mem. Soc. Astron. Ital., 77, 470
Mathis S., Palacios A., Zahn J.-P., 2004, A&A, 425, 243
Metcalfe T. S., Montgomery M. H., Kawaler S. D., 2003, MNRAS, 344, L88
Meynet G., Maeder A., 2000, A&A, 361, 101
Michaud G., Richard O., Richer J., VandenBerg D. A., 2004, ApJ, 606, 452
Miglio A., 2006, in Sterken C., Aerts C., eds, ASP Conf. Ser. Vol. 349, Astrophysics of Variable Stars. Astron. Soc. Pac., San Francisco, p. 297

Miglio A., Montalbán J., Noels A., 2006, Commun. Asteroseismol., 147, 89
Miglio A., Montalbán J., Dupret M.-A., 2007, MNRAS, 375, L21
Montalbán J., Théado S., Lebreton Y., 2007, in Straka C. W., Lebreton Y., Monteiro M. J. P. F. G., eds, EAS Publications Series Vol. 26, Comparisons for ESTA-Task 3: CLES and CESAM. EDP Sciences, Les Ulis, p. 167
Monteiro M. J. P. F. G., Thompson M. J., 2005, MNRAS, 361, 1187
Monteiro M. J. P. F. G., Christensen-Dalsgaard J., Thompson M. J., 1994, A&A, 283, 247
Montgomery M. H., Metcalfe T. S., Winget D. E., 2003, MNRAS, 344, 657
Moya A., Suárez J. C., Amado P. J., Martin-Ruíz S., Garrido R., 2005, A&A, 432, 189
Pamyatnykh A. A., 1999, Acta Astron., 49, 119
Pinsonneault M. H., Kawaler S. D., Sofia S., Demarque P., 1989, ApJ, 338, 424
Popielski B. L., Dziembowski W. A., 2005, Acta Astron., 55, 177
Press W. H., Teukolsky S. A., Vetterling W. T., Flannery B. P., 1992, Numerical Recipes in FORTRAN. The Art of Scientific Computing, 2nd edn. University Press, Cambridge
Ribas I., Jordi C., Giménez Á., 2000, MNRAS, 318, L55
Richard O., 2005, in Alecian G., Richard O., Vauclair S., eds, EAS Publications Series Vol. 17, Element Stratification in Stars: 40 Years of Atomic Diffusion. EDP Sciences, Les Ulis, p. 43
Richard O., Michaud G., Richer J., 2001, ApJ, 558, 377
Rieutord M., Dintrans B., 2002, MNRAS, 337, 1087
Rogers F. J., Iglesias C. A., 1992, ApJS, 79, 507
Schaller G., Schaerer D., Meynet G., Maeder A., 1992, A&AS, 96, 269
Scuflaire R., Montalbán J., Théado S., Bourge P.-O., Miglio A., Godart M., Thoul A., Noels A., 2007a, Ap&SS, in press (doi:10.1007/s10509-007-9577-6)
Scuflaire R., Théado S., Montalbán J., Miglio A., Bourge P.-O., Godart M., Thoul A., Noels A., 2007b, Ap&SS, in press (doi:10.1007/s10509-007-9650-1)
Seaton M. J., Badnell N. R., 2004, MNRAS, 354, 457
Straka C. W., Demarque P., Guenther D. B., 2005, ApJ, 629, 1075
Suárez J. C., Moya A., Martín-Ruíz S., Amado P. J., Grigahcène A., Garrido R., 2005, A&A, 443, 271
Tassoul M., 1980, ApJS, 43, 469
Unno W., Osaki Y., Ando H., Saio H., Shibahashi H., 1989, Nonradial Oscillations of Stars, 2nd edn. Univ. Tokyo Press, Tokyo
Waelkens C., 1991, A&A, 246, 453
Young P. A., Arnett D., 2005, ApJ, 618, 908
Zahn J.-P., 1991, A&A, 252, 179
Zima W., 2006, A&A, 455, 227

This paper has been typeset from a TEX/LATEX file prepared by the author.